Evaluation of a dual signal subspace projection algorithm in magnetoencephalographic recordings from patients with intractable epilepsy and vagus nerve stimulators

Chang Cai[a], Jiajing Xu[a], Jayabal Velmurugan[a,b,c,d], Robert Knowlton[g], Kensuke Sekihara[e,f], Srikantan S Nagarajan[a], Heidi Kirsch[a,g]

[a]*Department of Radiology and Biomedical Imaging, University of California, San Francisco, CA, USA 94143-0628 e-mail: sri@ucsf.edu*
[b]*Department of Clinical Neurosciences, National Institute of Mental Health and Neurosciences, Bangalore, India*
[c]*MEG Research Center, National Institute of Mental Health and Neurosciences, Bangalore, India*
[d]*Department of Neurology, National Institute of Mental Health and Neurosciences, Bangalore, India*
[e]*Department of Advanced Technology in Medicine, Tokyo Medical and Dental University, 1-5-45 Yushima, Bunkyo-ku, Tokyo 113-8519, Japan*
[f]*Signal Analysis Inc., Hachioji, Tokyo*
[g]*Department of Neurology, University of California, San Francisco, CA 94143-0628 e-mail: Heidi.Kirsch@ucsf.edu*

Abstract

Magnetoencephalography (MEG) data are subject to many sources of environmental noise, and interference rejection is a necessary step in the processing of MEG data. Large amplitude interference caused by sources near brain have been both common in clinical settings and difficult to reject. Artifacts from vagal nerve stimulators (VNS) are a common and difficult example. In this study, we describe a novel MEG interference rejection algorithm called dual signal subspace projection (DSSP) and evaluate its performance in clinical MEG data from people with epilepsy and implanted VNS. The performance of DSSP was evaluated in a retrospective cohort study of patients with epilepsy and VNS who had MEG scans for source localization of interictal epileptiform discharges. DSSP was applied to the MEG data and we evaluated the success of interference rejection based on visual inspection of the resulting signal and estimation of the location and time-course of observed interictal spikes, using an empirical Bayesian source reconstruction algorithm (Champagne). Clinical recordings, after DSSP processing, became more readable and more epileptic spikes could be clearly identified. Localization results significantly improved from those achieved before DSSP processing. With Champagne, when DSSP-processed data were used, there was a higher chance of successful spike localization, including meaningful estimates of activity time courses. The Champagne results using DSSP-processed data differed from those done prior to DSSP. Therefore,

DSSP is a valuable novel interference rejection algorithm that can be successfully deployed for the removal of strong artifacts and interferences in MEG.

Keywords:
Brain Mapping, Magnetoencephalography, DSSP, Intractable Epilepsy, Vagus Nerve Stimulators

1. Introduction

From the time of its first introduction, magnetoencephalography (MEG) has been used to map functional brain activity noninvasively with good spatial and excellent temporal resolution, and thus to offer valuable information for use in clinical neurology and basic neuroscience. However, MEG has suffered from an important shortcoming: it is prone to contamination from signals other than the signals of interest - including inevitable non-biological sources like power lines and trains, and biological sources outside of the brain like the heart. Though most of this interference is of similar magnitude to brain activity, some of it is high amplitude and needs special attention - including artifact from dental work, and especially interference from vagal nerve stimulators (VNS), relatively common in people with intractable epilepsy, that makes it very difficult for us to see and then to model activity of interest [1, 2, 3].

A variety of methods have been used to minimize artifact in magnetoencephalographic recordings with varying degrees of success. Averaging responses over trials is one method commonly used; this takes advantage of the idea that interference in different trials is statistically independent, whereas evoked signals are not. However, this method requires a large number of trials, and evoked signals must be relatively similar and robust [4]. Filtering is another widely applied method, but requires prior knowledge about the interference. Recently, data-driven approaches such as principal component analysis (PCA), independent component analysis (ICA) have been popular. However, these methods ask users to make subjective choices during application (e.g. choice of threshold in PCA and of interference component in ICA), and the methods cannot exploit pre-/poststimulus partitioning of the data [5, 6]. Joint decorrelation is another method commonly supposed to be robust to many types of interference problems, but its use requires the design of different bias filters for different interference types, and thus to some extent requires prior knowledge of the interference [7]. Algorithms based on statistical properties of the interference are a class of automated interference algorithm method hailed as both reliable and robust. The partitioned factor analysis (PFA) algorithm [1, 8, 9] is implemented by obtaining a probabilistic model from the data distributions in the pre-stimulus period (when the interference exists) and the post-stimulus period (when both interference and true signal exist), and then inferring model parameters from these distributions. This method handles most types of interference well, but since it relies on the availability of separate measurements that capture the statistical properties of the interference, its use is limited to situations where such separate measurements are appropriate, and it is not effective for

removing overlapped interference [4]. Also, these algorithms may not be effective for interference of extremely large magnitude relative to the signals being estimated, which is often seen in MEG data in patients with VNS implants.

Artifacts of significant magnitude are not rare in MEG recordings, and resolving MEG data from distorted recordings is often of great clinical significance. Particularly in the case of people with intractable epilepsy who have received VNS implants and have continued refractory focal onset seizures, MEG studies are an important part of the evaluation for and the planning of resective surgery. Without interference rejection, MEG data in many people with VNS implants will be completely distorted by significant artifact from the stimulator and the lead-wires, making it extremely difficult to see interictal epileptiform activity or stimulus evoked responses from primary sensory cortices, thus diminishing the usefulness of MEG for these patients and, thereby, their hope for recovery [3]. Therefore, developing and testing algorithms for interference rejection in MEG data is important, especially new algorithms that specifically address the kind of interference that is not well handled by currently available options but that is clinically important (e.g. VNS implant interference). Ideally such an algorithm would be robust and broadly capable of rejection of as many types of interference as possible. Given that many source localization platforms include lead fields, it would be ideal to offer a tool that is also based on lead fields. Right now options are restricted to specific hardware platforms. For example, the temporally extended signal space separation method (tSSS) developed by one MEG manufacturer offers a potential solution [10] but this tool has only been demonstrated for the Elekta platform and has not been shown for other platforms. In contrast, here we show a MEG hardware platform independent algorithm for large interference rejection.

Dual signal subspace projection (DSSP) is a newly proposed algorithm for removal of large interference in biomagnetic measurements, and has the potential to handle many different kinds of interference [3]. DSSP is based on the fact that MEG signal has both spatial and temporal properties. This allows us to define a signal subspace in the space domain, and another signal subspace in the time domain. We assume that the interference signal is present all the time across the whole signal subspace, either inside or outside the spatial-domain signal subspace, or both. In contrast, activity from the brain is presumed to exist only inside the spatial domain signal subspace. The DSSP algorithm first projects the columns of the measured data matrix onto the inside and outside of the spatial-domain signal subspace, creating two 'projected' data matrices. The intersection of the row spans of these two 'projected' matrices is then taken to be an estimate of the time-domain interference subspace, and artifact removal is carried out on the basis of this estimated interference subspace. Details of the DSSP algorithm have been published recently, but the performance of DSSP in assisting the identification and localization of epileptiform discharges has not been determined. In this paper we evaluate its ability in these arenas, using subject specific lead fields and selecting parameters, exploring its capability to handle various artifacts as part of processing of clinical datasets. In particular, we will evaluate whether it will be helpful to solve the problem of spike detec-

tion in patients with VNS implants. We will also test its ability to improve source localization of spikes using Champagne, an empirical Bayesian source reconstruction algorithm described previously [11].

2. Method

2.1. DSSP

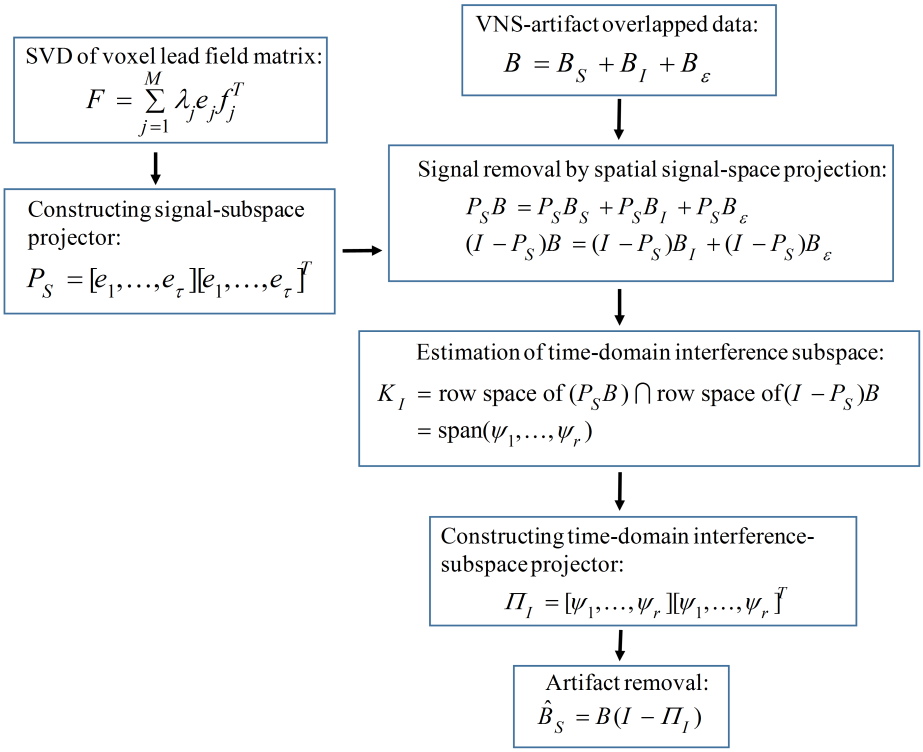

Figure 1: Schematic showing the processing steps of DSSP.

This section introduces the processing steps of DSSP briefly; details of the derivation can be found in Appendix A. Figure 1 shows the steps of DSSP. Firstly, we input the VNS-artifact overlapped data $\boldsymbol{B}_{M\times K}$ which consists of signal matrix $\boldsymbol{B}_S$, interference matrix $\boldsymbol{B}_I$ and noise matrix $\boldsymbol{B}_{\boldsymbol{\varepsilon}}$; At the same time we calculate the Singular Value Decomposition (SVD) of voxel lead field matrix and construct the signal-subspace projector $\boldsymbol{P}_S$. The DSSP algorithm then applies $\boldsymbol{P}_S$ and $\boldsymbol{I} - \boldsymbol{P}_S$ to the data matrix $\boldsymbol{B}$ to create two kinds of data matrices $\boldsymbol{P}_S\boldsymbol{B}$ and $(\boldsymbol{I} - \boldsymbol{P}_S)\boldsymbol{B}$. Next, DSSP estimates the time-domain interference subspace $\mathcal{K}_I$ and constructs the time-domain interference-subspace projector $\boldsymbol{\Pi}_I$. Lastly, interference removal is achieved and the signal matrix is estimated by the time-domain signal space projection $\widehat{\boldsymbol{B}}_S = \boldsymbol{B}(\boldsymbol{I} - \boldsymbol{\Pi}_I)$.

2.2. Subjects

We selected 10 epilepsy patients with VNS who underwent a clinical MEG study as part of epilepsy surgery evaluation at the University of California, San Francisco (UCSF) Biomagnetic Imaging Laboratory (BIL) between November 24th, 2004 and May 6th, 2016. Prior to MEG, all patients had high-resolution epilepsy protocol 3T T1-MRI scans for coregistration of dipoles. Table 1 summarizes clinical characteristics of these subjects.

2.3. MEG recordings

Simultaneous EEG and MEG recordings were performed inside a magnetically shielded room with a 275 channel whole-head axial gradiometer system (VSM MedTech, Port Coquitlam, British Columbia). MEG data were recorded from each patient in a passband of 0-75 Hz using a CTF 275 channel whole cortex MEG helmet while simultaneous twenty-one channel scalp EEG data were recorded using a modified international 10-20 system that includes subtemporal electrodes. Thirty to forty minutes of spontaneous data were obtained in intervals of 10-15 min with the patient asleep and awake. The position of the patient's head in the dewar relative to the MEG sensors was determined using indicator coils before and after each recording interval to verify adequate sampling of the entire field. The data were then bandpass filtered offline, initially at 1-70 Hz. More details of the recording methods have been previously described [4]. As artifact commonly distorted MEG recordings from the patients with VNS implants, in order to enable for visual analysis and dipole fitting of raw data, additional bandpass filters (typically 10-70 Hz or 20-70 Hz) were applied as needed during analysis of MEG data. After the application of DSSP for artifact removal, all data were bandpass filtered at 1-70 Hz.

2.4. Epileptic spike analysis

Spikes were visually identified by a certified EEG technologist (MM) and clinical neurophysiologist (JV) and were confirmed by a board-certified clinical neurophysiologist and epileptologist (HEK). EEG spikes were identified based on the criteria defined by the International Federation of Clinical Neurophysiology (IFCN) [12] and the ACMEGS [13] for EEG epileptiform discharges. MEG spikes were chosen for analysis based on duration ($< 80ms$), morphology, field map, and lack of associated artifact. The onset of each spike was marked as the rising deflection of the first sharp negativity from the baseline and equivalent current dipoles were fit using commercial software provided by CTF Systems (VSM MedTech, Port Coquitlam, British Columbia). Only localized spikes with a goodness of fit higher than 90% were accepted. Co-registration of dipoles to MRI scans was performed using fiducials (nasion and preauricular points) to produce magnetic source images (MSI) of dipoles superimposed on anatomic images. The fitted spike dipoles were then inspected and validated according to their location. Simultaneous EEG during MEG was used to define and confirm spikes on MEG, ascertaining that a signal was not an artifact or another physiologic feature, and also to identify spikes when MEG recordings were heavily

Table 1: Clinical characteristics of ten subjects. Note that some patients were referred from outside institutions and thus their information was limited to that available at the time of the MEG scan

ID	Age	Duration of Epilepsy	MR abnormality	Ictal EEG	Interictal EEG	PET CT	Presumed EZ	Interictal MEG spikes	Num of spikes before DSSP	Num of spikes after DSSP	Notes
1	22	18	Left lateral frontal lobe cortical dysplasia	Poorly localized; left frontocentral region	Left frontocentral spikes or polyspikes	Normal but PET fusion with MRI corresponding hypometabolism	Left frontal onset	Left frontotemporal	0	39	
2	25	20	Primary read as normal, secondary read as bilateral posterior pachygyria	Seizures arising independently from each hemisphere; poorly localized	Independent bitemporal spikes; generalized paroxysmal fast actvity	Negative	Unknown to date	Bilateral slow waves model bilaterally in the suprasylvian frontal and infra-sylvian temporal lobes	44	33	
3	44	32	Unremarkable	Not available	Right temporal sharp waves, generalized spike and polyspike discharges	N/A	Unknown to date	Right temporal, right frontal	107	168	
4	22	20	Encephalomalacia of the left temporal lobe, volume loss of left hippocampus	Left parietal region	Left TIRDA, frequent broad spikes over left temporo-parietal region, occasional left anterior temporal predominance	N/A	Left temporo-parietal-occipital	Posterior medial left temporal lobe	3	100	Patient had a posterior temporal resection and a subsequent additional occipital lobe resection 1 year later with success
5	17	Information not available	Left hipopcampal atrophy, left hemispheric cortical dysplasia	Left hemisphere onset	Intermittent left frontotemporal discharges	Hypometabolism of left temporal lobe, left parietal lobe, left posterior occiptal lobe	Left hemisphere, probable left temporal lobe	Left temporal region	47	143	
6	38	17	Left parietal, left temporal	Independent bilateral frontotemporal	Independent right and left temporal discharges	Bilateral temporal hypometabolism	Frontal or temporal; laterality unknown	None	5	14	
7	31	25	Unremarkable	Vertex spike followed by diffuse fast activity	Bilateral central/paracentral regions	N/A	Unknown to date	Right cingulate gyrus; L>R perirolandic regions	35	54	
8	37	19	T2/FLAIR hyperintensity and atrophy of bilateral temporal lobes, $L > R$	Left frontotemporal	Left anterior temporal; also rare right temporal spikes	Bilateral temporal hypometabolism	Left mesial temporal	Right temporal spikes, rare left temporal spikes	24	32	
9	26	Since young child	Expected changes from medial left frontal lobe corticectomy; otherwise unremarkable	Poorly localized and lateralized; some with preceding left parasagittal sharp waves	No interictal	N/A	Frontal; lateralization unclear but more likely left	None	43	72	
10	28	27	Left parietal cavernous malformation	Suggestive of frontal onset but poorly lateralized	Bifrontal sharp waves, left frontal spikes	Increased metabolic activity in high left posterior pariental sulcus	Unknown to date	Right suprasylvian frontal lobe	3	53	

contaminated by VNS artifact (ie when MEG data were significantly distorted, spike identification relied heavily on EEG).

2.5. DSSP performance evaluation

First, we evaluate the performance of DSSP with another interference removal method (Adaptive Noise Canceling, or ANC) which makes use of data from reference sensors. The reference sensors collect data containing interference but not the signal of interest [14, 15]. For this study, we define the reference sensor as the time course with the highest power where noise dominates. ANC also uses the idea of subspace projection, but it uses reference sensors to create the span of interference, then projects data from each sensor onto the subspace orthonormal to the span of interference so that interference specific to that sensor is eliminated, leaving sources of interest retained. Here, we compare the interference rejection performance of DSSP and of ANC by comparing the power spectral density (PSD) in each MEG channel after cleaning.

After DSSP implementation, cleaned MEG recordings were analyzed as described above (without additional band pass filtering) by three individuals with expertise in interictal spike detection (MM, JV, HEK) who were blinded to the results of the initial (pre-DSSP) analysis. The results were then compared with the original analysis and included quantification of the number of spikes identified and localized, and concordance with other clinical information (EEG, semiology, MRI lesion if present).

Finally, DSSP was integrated into a newer source localization pipeline: a united Bayesian framework for MEG/EEG source imaging that includes Variational Bayes Factor Analysis (VBFA) for noise approximation and a Sparse Bayesian Algorithm (Champagne) for source localization [16, 17], to see whether localization improved upon the incorporation of DSSP algorithm. For each case studied, ten representative spikes seen well on EEG but poorly on MEG in the unprocessed recordings were selected for analysis. For each of the spike selections, Champagne was run for 300 ms (i.e. using 180 data points) on truncated MEG epochs each centered on the selected spike; the required noise estimate input for Champagne was obtained by running VBFA on the 1s of MEG preceding the truncated epoch. The spike source reconstruction map obtained after implementing Champagne was used to judge the performance of DSSP: we observed the activation value of the localized spike activity and the recovered activity time-series, and compared these with standard clinical spike mapping as described above, as well as with correlative clinical data.

3. Results

Figure 2 shows EEG data (a) and MEG data (b) from a patient with intractable epilepsy and a VNS implant. It features VNS artifact with partial periodicity, low frequency and high amplitude. After DSSP is applied, as shown in (c), this periodic feature is greatly diminished and the background looks similar to that of most people with epilepsy who do not have VNS. Figure 3 shows similar data for another patient.

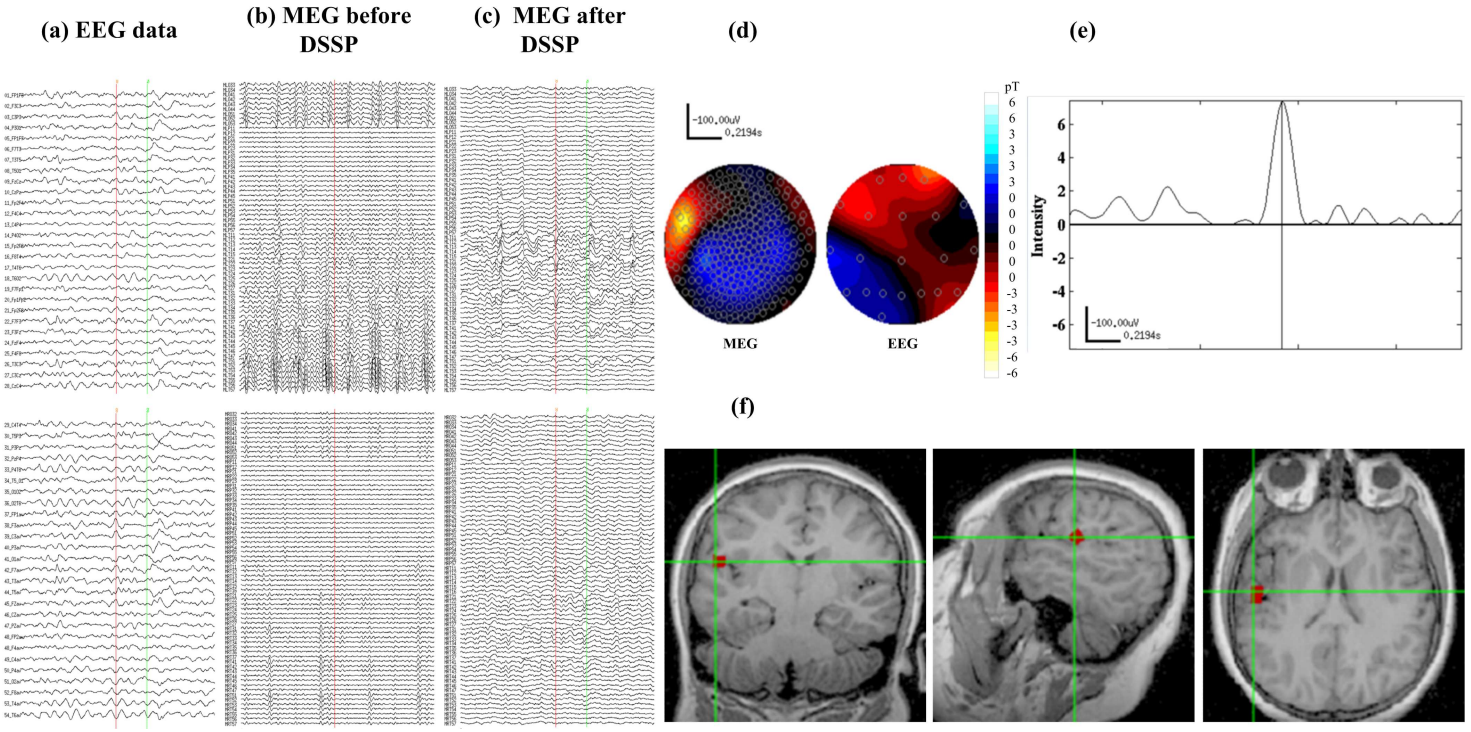

Figure 2: A representative case showing the effect of the application of DSSP (Subject 5 from Table 1). (a) EEG epoch corresponding to MEG epoch (selected channels) (b) Raw MEG recordings (selected channels) (c) DSSP-processed MEG data. The red line marks a spike not identified in the raw data but seen in the DSSP-processed data, the green line in (a) and (c) mark another spike. (d) Field maps for MEG (after DSSP) and EEG. (e) Time series for the spike of interest reconstructed through Champagne. (f) spike localization using Champagne on DSSP-processed data.

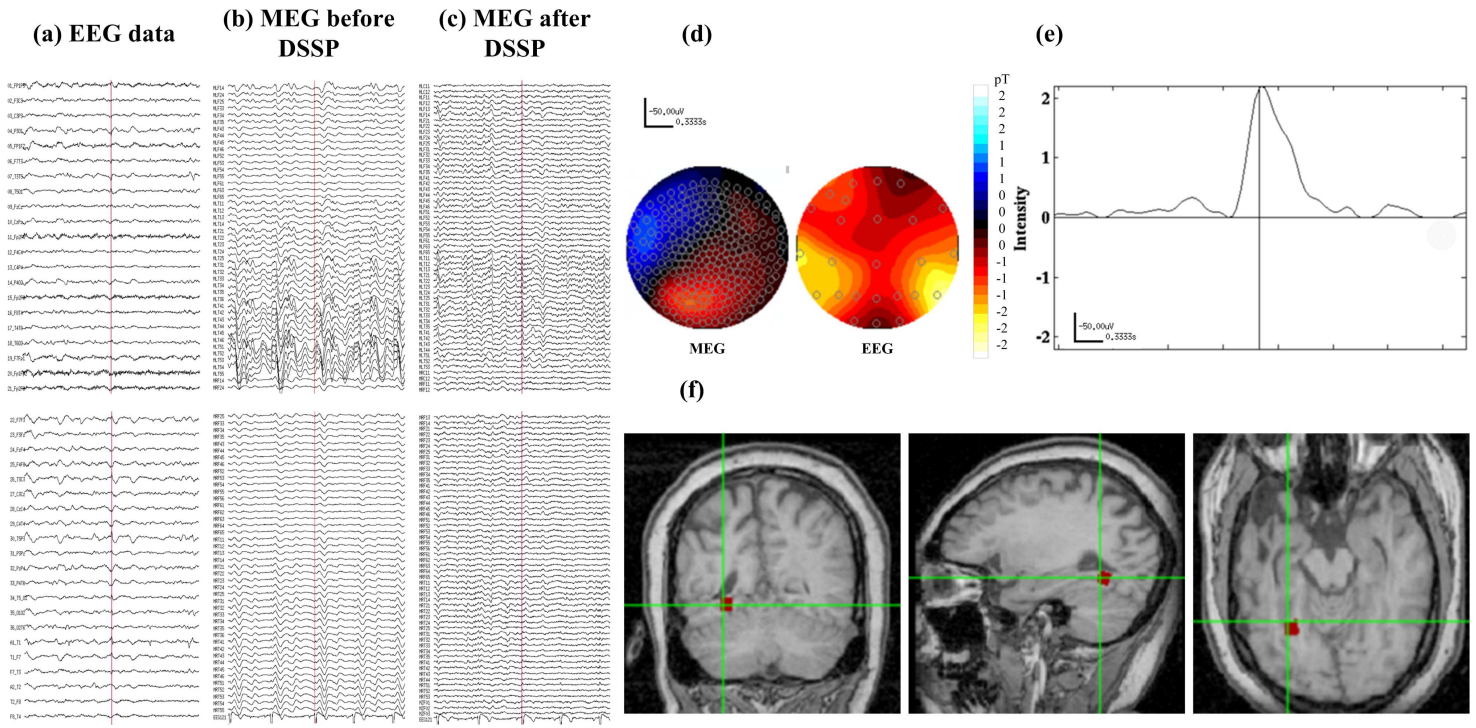

Figure 3: Another representative case (Subject 4 from Table 1) (a) EEG epoch corresponding to MEG epoch (selected channels) (b) Raw MEG recordings (selected channels) (c) DSSP-processed MEG data. The red line marks a spike not identified in the raw data but seen in the DSSP-processed data. (d) Field maps for MEG (after DSSP) and EEG. (e) Time series for the spike of interest reconstructed through Champagne. (f) spike localization using Champagne on DSSP-processed data.

3.1. DSSP vs ANC

Figure 4 shows power spectral density of the ten subjects before and after artifact removal using DSSP and ANC. As is shown, compared to the raw VNS datasets, the PSD decreases after DSSP and ANC, especially for low frequency bands from 0 to 30 Hz, while for high frequency bands, the PSD is the same as the raw datasets for both DSSP- and ANC-cleaned data. In addition, DSSP removes more low frequency power than does ANC.

Figure 5 shows the PSD of all channels for ten subjects with VNS implanted before and after artifact removal by DSSP and ANC. As we can see, compared the PSD for raw signal, PSD after DSSP is reduced in all channels; while for data processed with ANC, some channels have the same PSD as the raw datasets. The PSD for all channels is reduced more by DSSP than by ANC.

3.2. Visual analysis and source localization

After the application of the DSSP algorithm to MEG data from people with intractable epilepsy and VNS, spikes could be visually identified from MEG background at a high rate, both spikes that were well seen on EEG and those seen primarily on MEG. Figure 6 shows the average number of spikes that could be identified by visual inspection of the MEG and the average number of spikes that could be localized by topographical inspection before and after DSSP. As is shown, over twice as many spikes could be identified after DSSP ($70.8/31.1 = 2.3$), and over four times as many spikes could be localized after DSSP ($45.6/11 = 4.15$). The percentage of spikes that could be localized improved from 35.37% (11/31.1) before DSSP to 64.41% (45.6/70.8) after DSSP. DSSP improves the rate of spike identification and source localization.

3.3. Champagne algorithm

Directly running Champagne on MEG recordings that are distorted by VNS artifact resulted in localization failure in nine out of the ten cases; either no strong activation could be found, or the activity was localized to unusual positions (e.g. near or outside of the skull), and the activity time-series recovered did not resemble a spike. On the other hand, when DSSP was incorporated prior to Champagne, the localization results were markedly improved. As is shown in Figure 7, all cases could be localized correctly with DSSP. We performed a Chi-Square test comparing numbers of successful and unsuccessful localizations before and after DSSP, which give us $\chi^2 = 16.364$ and $p(\chi^2 > 16.364) = 0.0001$. Localizations were clearer and in plausible brain areas, and meaningful spike-like time-series were recovered. Figures 2(d) and 3(d) show field maps for MEG after DSSP and EEG maps, Figures 2(e) and 3(e) show respective Champagne time series for the spike of interest in the two cases previously discussed, and Figures 2(f) and 3(f) show source localization. In summary, the chance that a given spike from a VNS-contaminated record could be successfully localized using the Champagne algorithm greatly increased with DSSP pre-processing.

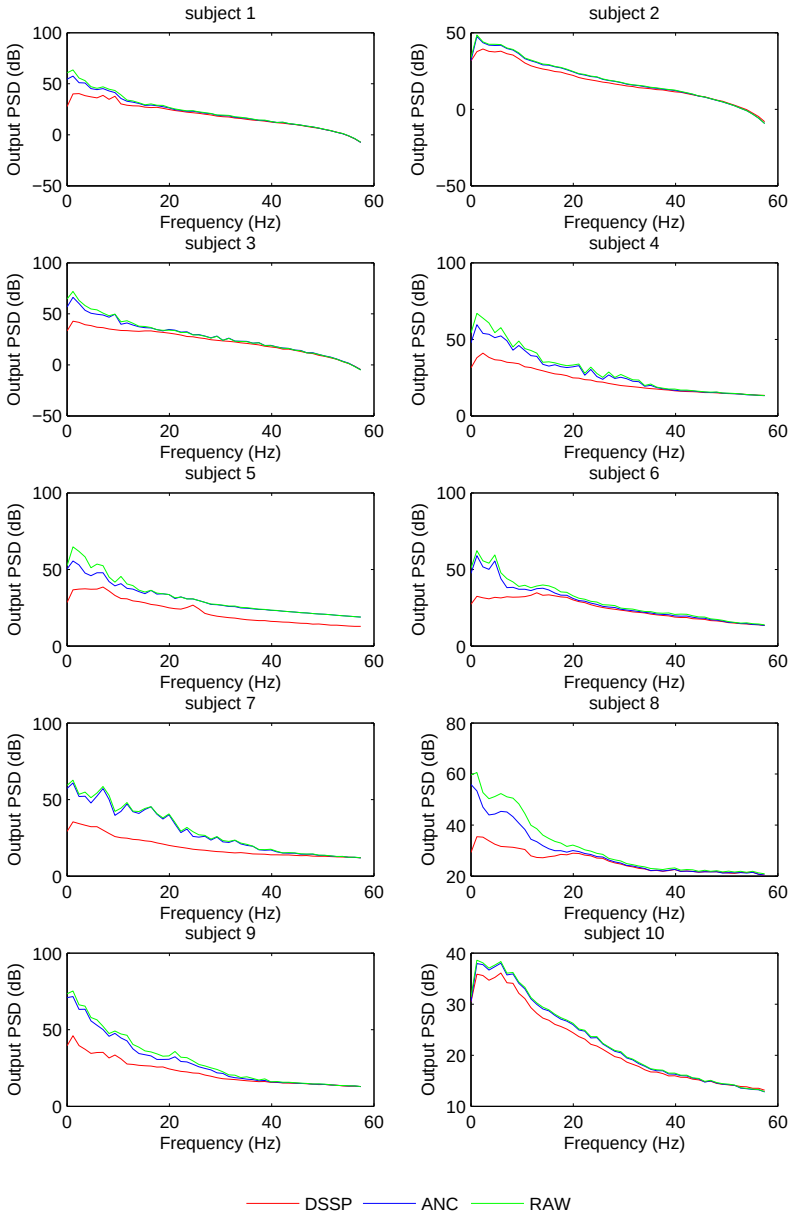

Figure 4: Power Spectral Density (PSD) comparison of DSSP and ANC for 10 subjects.

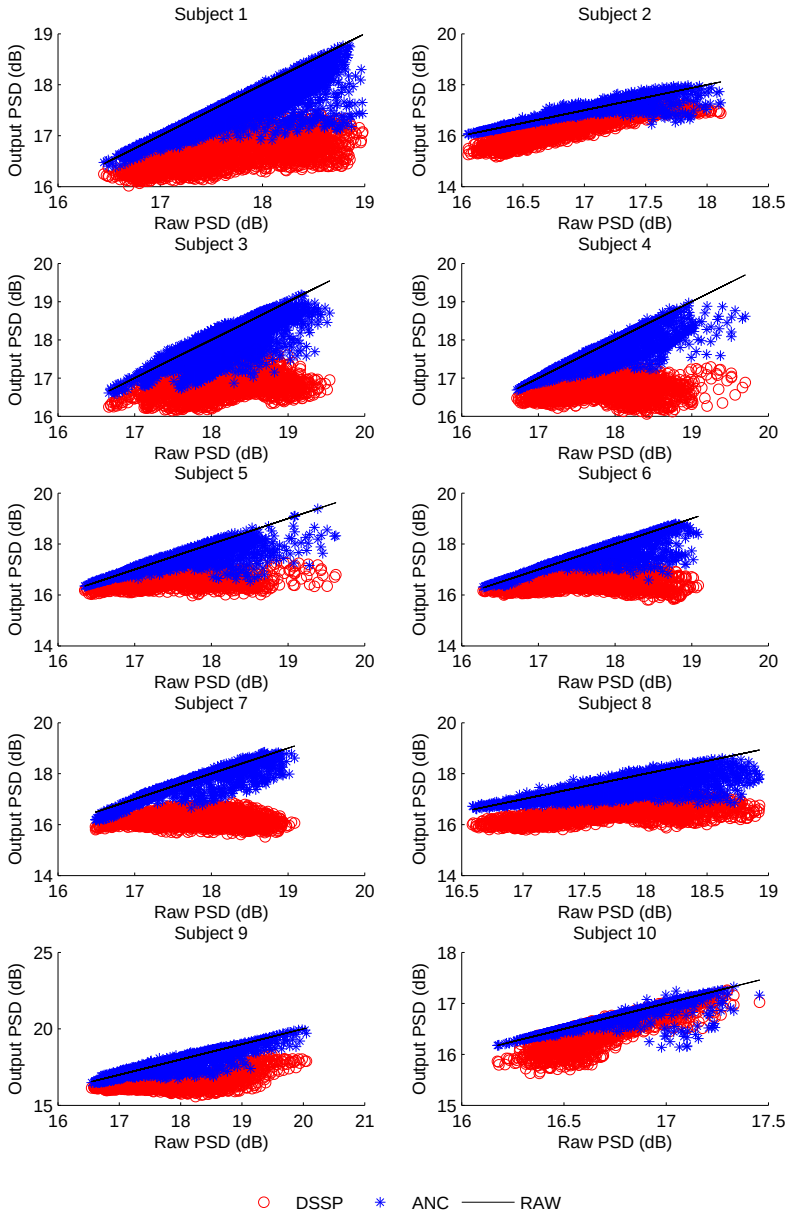

Figure 5: Power Spectral Density (PSD) across channels after DSSP and after ANC for ten subjects.

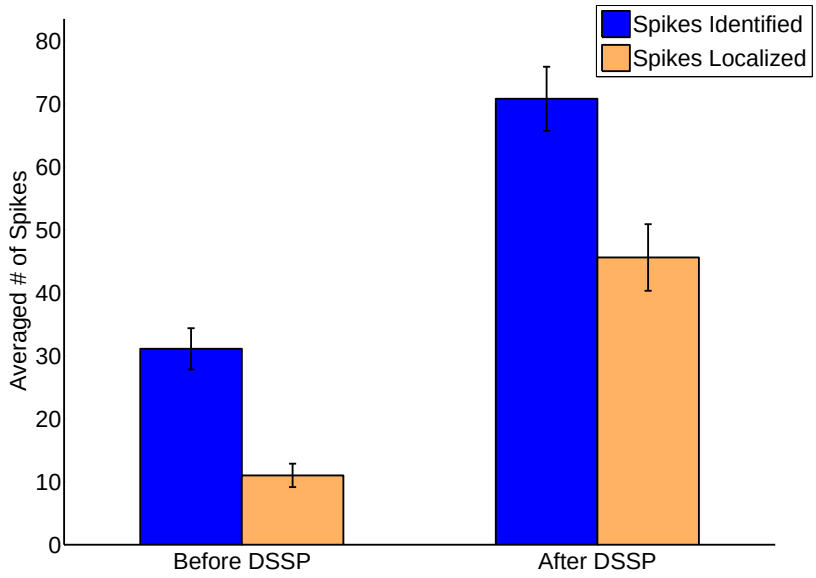

Figure 6: The averaged number of spikes that could be identified by visual inspection and localized by topographical inspection before and after the application of DSSP for ten subjects with standard error bars.

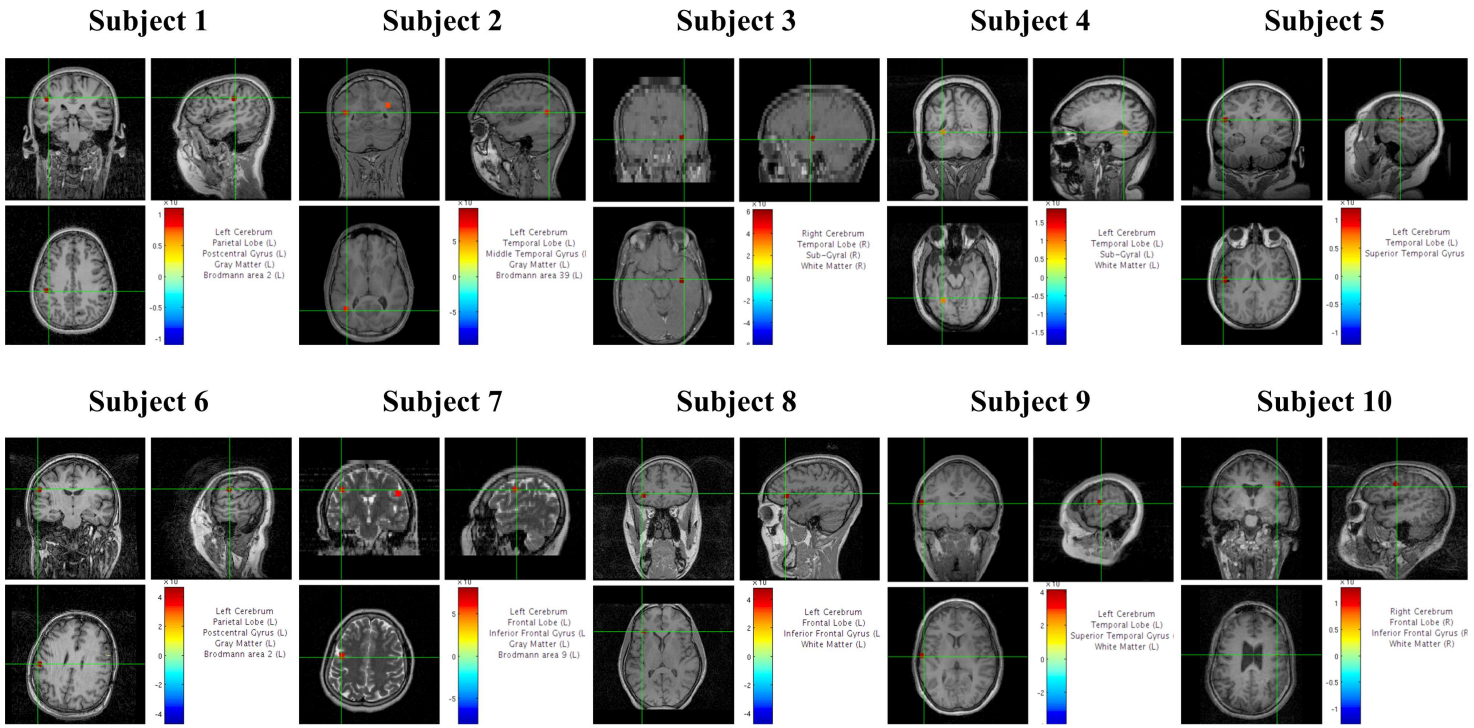

Figure 7: Source localization results for all ten subjects using Champagne after DSSP.

4. Discussion

In this study, DSSP is evaluated using typical clinical data from people with epilepsy and VNS, showing its potential to diminish the influence of interference. Compared to classical adaptive noise cancelling (ANC), both DSSP and ANC retain the PSD of the MEG signal in high frequency bands, but DSSP reduces more PSD over lower frequency bands. Additionally, DSSP processing of MEG data enabled better visual identification of spikes, making meaningful the MEG recordings that were contaminated and previously of limited value. Finally, when integrated with the Champagne source reconstruction algorithm, DSSP did help to achieve more reasonable spike localizations and meaningful recovered spike activity time series. The successful rejection of VNS artifact using DSSP should enable improved treatment (including surgical planning for resection or other localized therapies) of people with intractable epilepsy and VNS. Given these results, as we gain further experience with DSSP, its potential use in the setting of other interference types can also be explored.

There are several limitations to this study. First, small sample size could potentially limit the generalizability of our results. However, we included all patients who had VNS implants in our study. Second, the neurophysiologists who examined the post DSSP data were blinded to the results of the original analysis, there may be some bias due to spike identification in cleaner MEG data. Nevertheless, our localization findings suggest that this bias is not severe. Third, this is a retrospective and non-randomized study. Currently, for new cases with VNS artifact, we are undertaking a prospective study applying DSSP prior to initial analysis, and results of this prospective study will be published in the future. Finally, although better localization was achieved with the addition of DSSP to Champagne, whether this truly improved the accuracy of epileptogenic zone mapping is unknown. Most of time the Champagne localization results differed from those obtained using the single equivalent dipole fitting method, though the difference mostly lay within one brain functional zone, and though the results of both techniques matched the primary clinical diagnosis. Additional information about the true epileptogenic zone (e.g. from follow-up after resective surgery) will be needed to make such judgment. Therefore, we can only conclude that DSSP helps achieve spike mapping, but cannot evaluate localization accuracy. We are collecting follow-up information from patients who went through surgery after MEG recording, and in future this information could be used as a gold standard to judge the performance of DSSP.

5. Conclusion

In short, DSSP is a novel interference rejection algorithm worth exploration. The retrospective clinical study has shown its potential to deal with high amplitude, periodic interference currently not handled well by other algorithms. DSSP helped to recover distorted MEG recordings from people with intractable epilepsy and VNS implants, making epileptic spike identification easier and spike mapping better. The specificity of this improved spike mapping is still unknown.

Acknowledgment

The authors would like to thank Susanne Honma, Danielle Mizuiri and Anne Findlay for collecting much of the MEG data in the Biomagnetic Imaging Laboratory. We would also like to thank Mary Mantle for blinded analysis of some of the MEG data. This work was supported by NIH grants R01EB022717, R01DC013979, UCOP MRP-17-454755, and a gift from Ricoh Company Ltd..

Appendix A. Derivation of DSSP

Appendix A.1. Data model

This section briefly describes the DSSP algorithm. A full explanation of the algorithm is available in [3]. Also, a detailed explanation of the DSSP algorithm in the context of the time-domain signal subspace can be found in [18]. Let us define the measurement of the m-th sensor at time t as $y_m(t)$. The measurement from the whole sensor array is expressed as a column vector $\boldsymbol{y}(t)$: $\boldsymbol{y}(t) = [y_1(t), y_2(t), \ldots, y_M(t)]^T$, which is called the data vector. Here, M is the number of sensors, and the superscript T indicates the matrix transpose. Let us assume that a unit-magnitude source exists at $\boldsymbol{r}$ ($\boldsymbol{r} = (x, y, z)$). When this unit-magnitude source is directed in the x, y, and z directions, the outputs of the m-th sensor are respectively denoted as $l_m^x(\boldsymbol{r})$, $l_m^y(\boldsymbol{r})$, and $l_m^z(\boldsymbol{r})$. Let us define an $M \times 3$ matrix $\boldsymbol{L}(\boldsymbol{r})$ whose m-th row is equal to a 1×3 row vector $[l_m^x(\boldsymbol{r}), l_m^y(\boldsymbol{r}), l_m^z(\boldsymbol{r})]$. This matrix $\boldsymbol{L}(\boldsymbol{r})$, referred to as the lead field matrix, represents the sensitivity of the sensor array at $\boldsymbol{r}$.

The DSSP algorithm was proposed in order to remove interfering magnetic fields overlapped onto signal magnetic fields. The algorithm assumes the data model:

$$\boldsymbol{y}(t) = \boldsymbol{y}_S(t) + \boldsymbol{y}_I(t) + \boldsymbol{\varepsilon}, \tag{A.1}$$

where $\boldsymbol{y}_S(t)$, (called the signal vector), represents the signal of interest, $\boldsymbol{y}_I(t)$, (called the interference vector), represents the interference magnetic field, and $\boldsymbol{\varepsilon}$, (called the random vector), represents additive sensor noise. We denote the time series outputs of a sensor array $\boldsymbol{y}(t_1), \ldots, \boldsymbol{y}(t_K)$, where K is the total number of measured time points. The measured data matrix $\boldsymbol{B}$ is thus defined as: $\boldsymbol{B} = [\boldsymbol{y}(t_1), \ldots, \boldsymbol{y}(t_K)]$. The signal matrix is defined as $\boldsymbol{B}_S = [\boldsymbol{y}_S(t_1), \ldots, \boldsymbol{y}_S(t_K)]$, and the interference matrix as $\boldsymbol{B}_I = [\boldsymbol{y}_I(t_1), \ldots, \boldsymbol{y}_I(t_K)]$. Then, the data model in Eq. (A.1) is expressed in a matrix form as:

$$\boldsymbol{B} = \boldsymbol{B}_S + \boldsymbol{B}_I + \boldsymbol{B}_{\boldsymbol{\varepsilon}}, \tag{A.2}$$

where $\boldsymbol{B}_{\boldsymbol{\varepsilon}}$ is the noise matrix whose j-th column is equal to the noise vector $\boldsymbol{\varepsilon}$ at time t_j.

Appendix A.2. Pseudo-signal subspace projector

The dual signal space projection (DSSP) algorithm assumes that the interference sources are located outside the source space which indicates a region in which signal sources can exist. The DSSP algorithm uses the so-called pseudo-signal subspace projector, and to derive it, voxels are defined over the source space, in which the voxel locations are denoted $\boldsymbol{r}_1, \ldots, \boldsymbol{r}_N$. The augmented leadfield matrix over these voxel locations is defined as

$$\boldsymbol{F} = [\boldsymbol{L}(\boldsymbol{r}_1), \ldots, \boldsymbol{L}(\boldsymbol{r}_N)], \tag{A.3}$$

and the pseudo-signal subspace $\breve{\mathcal{E}}_S$ is defined such that

$$\breve{\mathcal{E}}_S = \mathrm{csp}(\boldsymbol{F}), \tag{A.4}$$

where the notation $\mathrm{csp}(\boldsymbol{X})$ indicates the column space of a matrix $\boldsymbol{X}$. If the voxel interval is sufficiently small and voxel discretization errors are negligible, we have the relationship $\breve{\mathcal{E}}_S \supset \mathcal{E}_S$ where $\mathcal{E}_S$ indicates the true signal subspace. Therefore, a vector contained in the signal subspace is also contained in the pseudo-signal subspace.

Let us derive the orthonormal basis vectors of the pseudo-signal subspace. To do so, we compute the singular value decomposition of $\boldsymbol{F}$:

$$\boldsymbol{F} = \sum_{j=1}^{M} \lambda_j \boldsymbol{e}_j \boldsymbol{f}_j^T, \tag{A.5}$$

where $\boldsymbol{e}_j$ and $\boldsymbol{f}_j$ are left and right singular vectors. In Eq. (A.5), we assume the relationship $M < N$, and the singular values are numbered in decreasing order. If the singular values $\lambda_1, \ldots, \lambda_\tau$ are distinctively large and other singular values $\lambda_{\tau+1}, \ldots, \lambda_M$ are nearly equal to zero, the leading τ singular vectors $\boldsymbol{e}_1, \ldots, \boldsymbol{e}_\tau$ form orthonormal basis vectors of the pseudo-signal subspace $\breve{\mathcal{E}}_S$. Thus, the projector onto $\breve{\mathcal{E}}_S$ is obtained using

$$\boldsymbol{P}_S = [\boldsymbol{e}_1, \ldots, \boldsymbol{e}_\tau][\boldsymbol{e}_1, \ldots, \boldsymbol{e}_\tau]^T. \tag{A.6}$$

Note that $(\boldsymbol{I} - \boldsymbol{P}_S)\boldsymbol{y}_S(t) = (\boldsymbol{I} - \boldsymbol{P}_S)\boldsymbol{B}_S = 0$ holds.

Appendix A.3. DSSP algorithm

The DSSP algorithm applies $\boldsymbol{P}_S$ and $\boldsymbol{I} - \boldsymbol{P}_S$ to the data matrix $\boldsymbol{B}$ to create two kinds of data matrices:

$$\boldsymbol{P}_S\boldsymbol{B} = \boldsymbol{B}_S + \boldsymbol{P}_S\boldsymbol{B}_I + \boldsymbol{P}_S\boldsymbol{B}_{\boldsymbol{\varepsilon}}, \tag{A.7}$$

$$(\boldsymbol{I} - \boldsymbol{P}_S)\boldsymbol{B} = (\boldsymbol{I} - \boldsymbol{P}_S)\boldsymbol{B}_I + (\boldsymbol{I} - \boldsymbol{P}_S)\boldsymbol{B}_{\boldsymbol{\varepsilon}}. \tag{A.8}$$

Let us use the notation $\mathrm{rsp}(\boldsymbol{X})$ to indicate the row space of a matrix $\boldsymbol{X}$. Then, the relationships, $\mathrm{rsp}(\boldsymbol{P}_S\boldsymbol{B}_I) = \mathcal{K}_I$, $\mathrm{rsp}((\boldsymbol{I} - \boldsymbol{P}_S)\boldsymbol{B}_I) = \mathcal{K}_I$, and $\mathrm{rsp}(\boldsymbol{B}_S) = \mathcal{K}_S$ hold, where $\mathcal{K}_S$ and $\mathcal{K}_I$ respectively indicate the time-domain signal and

interference subspaces. According to arguments in [18], we can finally derive the relationship:

$$\mathcal{K}_I \supset \mathrm{rsp}(\boldsymbol{P}_S\boldsymbol{B}) \cap \mathrm{rsp}((\boldsymbol{I}-\boldsymbol{P}_S)\boldsymbol{B}). \tag{A.9}$$

The equation above shows that the intersection between $\mathrm{rsp}(\boldsymbol{P}_S\boldsymbol{B})$ and $\mathrm{rsp}((\boldsymbol{I}-\boldsymbol{P}_S)\boldsymbol{B})$ forms a subset of the interference subspace $\mathcal{K}_I$. The basis vectors of the intersection can be derived using the algorithm described in [19]. Once the orthonormal basis vectors of the intersection $\boldsymbol{\psi}_1, \ldots, \boldsymbol{\psi}_r$ are obtained, we can compute the projector onto the intersection $\boldsymbol{\Pi}_I$ such that

$$\boldsymbol{\Pi}_I = [\boldsymbol{\psi}_1, \ldots, \boldsymbol{\psi}_r][\boldsymbol{\psi}_1, \ldots, \boldsymbol{\psi}_r]^T. \tag{A.10}$$

Using this $\boldsymbol{\Pi}_I$ as the projector onto the (time-domain) interference subspace $\mathcal{K}_I$, the interference removal is achieved and the signal matrix is estimated by the time-domain signal space projection[18], which is

$$\widehat{\boldsymbol{B}}_S = \boldsymbol{B}(\boldsymbol{I}-\boldsymbol{\Pi}_I) = \boldsymbol{B}(\boldsymbol{I}-[\boldsymbol{\psi}_1, \ldots, \boldsymbol{\psi}_r][\boldsymbol{\psi}_1, \ldots, \boldsymbol{\psi}_r]^T). \tag{A.11}$$

The method of removing the interference in a manner described above is called dual signal space projection (DSSP). Note that since the basis vectors of the intersection, $\boldsymbol{\psi}_1, \ldots, \boldsymbol{\psi}_r$, span only a subset of the interference subspace $\mathcal{K}_I$, this method cannot perfectly remove interferences. However, when the intersection $\mathrm{rsp}(\boldsymbol{P}_S\boldsymbol{B}) \cap \mathrm{rsp}((\boldsymbol{I}-\boldsymbol{P}_S)\boldsymbol{B})$ is a reasonable approximation of $\mathcal{K}_I$, interferences can effectively be removed by the DSSP algorithm.

References

[1] Srikantan S Nagarajan, Hagai T Attias, Kenneth E Hild II, and Kensuke Sekihara. A graphical model for estimating stimulus-evoked brain responses from magnetoencephalography data with large background brain activity. *NeuroImage*, 30(2):400–416, 2006.

[2] Samu Taulu and Juha Simola. Spatiotemporal signal space separation method for rejecting nearby interference in meg measurements. *Physics in Medicine & Biology*, 51(7):1759, 2006.

[3] Kensuke Sekihara, Yuya Kawabata, Shuta Ushio, Satoshi Sumiya, Shigenori Kawabata, Yoshiaki Adachi, and Srikantan S Nagarajan. Dual signal subspace projection (dssp): a novel algorithm for removing large interference in biomagnetic measurements. *Journal of neural engineering*, 13(3):036007, 2016.

[4] Srikantan S Nagarajan, Hagai T Attias, Kenneth E Hild, and Kensuke Sekihara. A probabilistic algorithm for robust interference suppression in bioelectromagnetic sensor data. *Statistics in medicine*, 26(21):3886–3910, 2007.

[5] A Ossadtchi, S Baillet, JC Mosher, D Thyerlei, W Sutherling, and RM Leahy. Automated interictal spike detection and source localization in magnetoencephalography using independent components analysis and spatio-temporal clustering. *Clinical Neurophysiology*, 115(3):508–522, 2004.

[6] Srikantan S Nagarajan, Hagai T Attias, Kensuke Sekihara, and Kenneth E Hild. Partitioned factor analysis for interference suppression and source extraction. In *International Conference on Independent Component Analysis and Signal Separation*, pages 189–197. Springer, 2006.

[7] Alain de Cheveigné and Lucas C Parra. Joint decorrelation, a versatile tool for multichannel data analysis. *Neuroimage*, 98:487–505, 2014.

[8] S. S. Nagarajan, H. T. Attias, K. Ee. Hild, and K. Sekihara. A probabilistic algorithm for robust interference suppression in bioelectromagnetic sensor data. *Statistics in Medicine*, 26:3886–910, 2007.

[9] Johanna M Zumer, Hagai T Attias, Kensuke Sekihara, and Srikantan S Nagarajan. Probabilistic algorithms for meg/eeg source reconstruction using temporal basis functions learned from data. *NeuroImage*, 41(3):924–940, 2008.

[10] Samu Taulu and Riitta Hari. Removal of magnetoencephalographic artifacts with temporal signal-space separation: demonstration with single-trial auditory-evoked responses. *Human brain mapping*, 30(5):1524–1534, 2009.

[11] Julia P Owen, David P Wipf, Hagai T Attias, Kensuke Sekihara, and Srikantan S Nagarajan. Performance evaluation of the champagne source reconstruction algorithm on simulated and real M/EEG data. *Neuroimage*, 60(1):305–323, 2012.

[12] Günther Deuschl, Andrew Eisen, et al. Recommendations for the practice of clinical neurophysiology: guidelines of the international federation of clinical neurophysiology. 1999.

[13] Anto I Bagic, Robert C Knowlton, Douglas F Rose, John S Ebersole, ACMEGS Clinical Practice Guideline (CPG) Committee, et al. American clinical magnetoencephalography society clinical practice guideline 1: recording and analysis of spontaneous cerebral activity. *Journal of Clinical Neurophysiology*, 28(4):348–354, 2011.

[14] Bernard Widrow, John R Glover, John M McCool, John Kaunitz, Charles S Williams, Robert H Hearn, James R Zeidler, JR Eugene Dong, and Robert C Goodlin. Adaptive noise cancelling: Principles and applications. *Proceedings of the IEEE*, 63(12):1692–1716, 1975.

[15] Y Adachi, M Shimogawara, M Higuchi, Y Haruta, and M Ochiai. Reduction of non-periodic environmental magnetic noise in meg measurement by continuously adjusted least squares method. *IEEE Transactions on Applied Superconductivity*, 11(1):669–672, 2001.

[16] David Wipf and Srikantan Nagarajan. A unified bayesian framework for MEG/EEG source imaging. *NeuroImage*, 44(3):947–966, 2009.

[17] David P Wipf, Julia P Owen, Hagai T Attias, Kensuke Sekihara, and Srikantan S Nagarajan. Robust bayesian estimation of the location, orientation, and time course of multiple correlated neural sources using MEG. *NeuroImage*, 49(1):641–655, 2010.

[18] K. Sekihara and S. S. Nagarajan. Subspace-based interference removal methods for a multichannel biomagnetic sensor array. *Journal of Neural Engineering*, 14(5):051001, 2017.

[19] Gene H Golub and Charles F Van Loan. *Matrix computations*, volume 3. The Johns Hopkins University Press, 2012.